ChemistryOpen

Research Article
doi.org/10.1002/open.202200176

Chemistry Europe
European Chemical Societies Publishing

www.chemistryopen.org

Cd²⁺ and Zn²⁺ Complexes with 2,4,6-Tri(2-pyridyl)-s-Triazine and Terephthalate for Rapid, High-Capacity Adsorption of Congo Red

Yanfang Zhao,[a, b] Yongliang Zhao,[a] Ziyang Guo,[a] Dan Zhou,[a] Shuai Yuan,[c] Xueqiong Zhang,*[d] and Haibin Chu*[a]

Three crystal complexes were designed and synthesised through the solvothermal method, with Cu²⁺, Zn²⁺, and Cd²⁺ ions as the metal centres and 2,4,6-tri(2-pyridyl)-s-triazine (TPTZ) and terephthalate (BDC²⁻) as the ligands. Their compositions were determined to be Cd(TPTZ)Cl₂ (Cd-MOF), {[Zn-(TPTZ)(BDC)]·3H₂O}ₙ (Zn-MOF), and Cu₂(PCA)₂(BDC)(H₂O)₂ (Cu-MOF) (PCA⁻ = 2-pyridinium amide), respectively. Cd-MOF can adsorb 90% of Congo red (CR) in 10 s at room temperature and atmospheric pressure, and CR removal was complete at 20 s over a wide pH range. The adsorption capacity for CR reached 1440 mg g⁻¹ in 5 min. Selective adsorption was demonstrated in mixed dyes. The adsorption kinetic data agree well with the pseudo-second-order kinetic model. The Temkin model was successfully used to evaluate the adsorption isotherms of CR on Cd-MOF at room temperature, suggesting that adsorption occurs through a hybrid of monolayer and multilayer mechanisms.

Introduction

Environmental pollution can cause human diseases including cancer.[1,2] Organic dyes as a class of pollutants can be released from papermaking, plastics, textiles, coatings, dyeing, rubber production, and other industries. Numerous approaches have been developed to remove organic dyes from aqueous solution, such as adsorption, filtration, catalytic degradation, electrostatic induction, ion exchange, photocatalysis, and so on.[3–8] Among them, adsorption has a low cost, high efficiency, simple operation, and almost harmless by-products.[9–12] A large variety of materials including natural materials,[13] clays,[14] fibres,[15] activated carbons,[16] zeolites,[17] metal oxide nanostructures,[18–20] graphene oxide,[21] metal-organic framework (MOF),[22–24] and covalent organic framework (COF)[25] have been applied to adsorbents, and some of them showed excellent adsorption capacity. In transition metal complexes with aromatic carboxylic acids and nitrogen heterocyclic ring compounds, micropores and exposed amino groups are known to facilitate selective adsorption of gases and organic dye molecules.[9,26–32] Depending on their electron configurations and radii, different transition metal ions may influence the composition, structure, and properties of the formed crystal complexes. Aromatic carboxylic acids, particularly terephthalic acid (H₂BDC), have been widely used as a bridge or a connecting agent in the synthesis of polymer network structures,[23,28,34] because they can link the metal ions to form frameworks or new polymers. 2,4,6-Tri(2-pyridyl)-s-triazine (TPTZ) is a nitrogen heterocycle. When combined with metal ions, it produces not only five-membered rings to increase the stability[35] but also the right spacing for framework structures or polymers.[36–38] Especially, the numerous exposed nitrogen atoms in TPTZ facilitate the adsorption of pollutants.

In this paper, we selected three transition metal ions Cu²⁺, Zn²⁺, and Cd²⁺ as the central ion, H₂BDC as a cross-linking ligand, and TPTZ as a nitrogen-containing aromatic ring ligand. The three designed and synthesised crystal complexes (Cd-MOF, Zn-MOF, and Cu-MOF) differ completely in their composition and structure (Scheme 1). We further studied their adsorption performance for Congo red (CR), rhodamine B (RB), methyl orange (MO), methylene blue (MB), and their mixtures. The results indicated that these complexes also have very different adsorption performance. The selective adsorption of CR was also investigated using a simulated organic waste liquid containing CR. In addition, we studied the adsorption under different pH. The results showed that the composition and structure of the crystal complexes strongly affect their adsorption properties. Cd-MOF and Zn-MOF can selectively adsorb CR

[a] Y. Zhao, Prof. Y. Zhao, Z. Guo, D. Zhou, Prof. Dr. H. Chu
     College of Chemistry and Chemical Engineering
     Inner Mongolia University
     Hohhot 010021 (P. R. China)
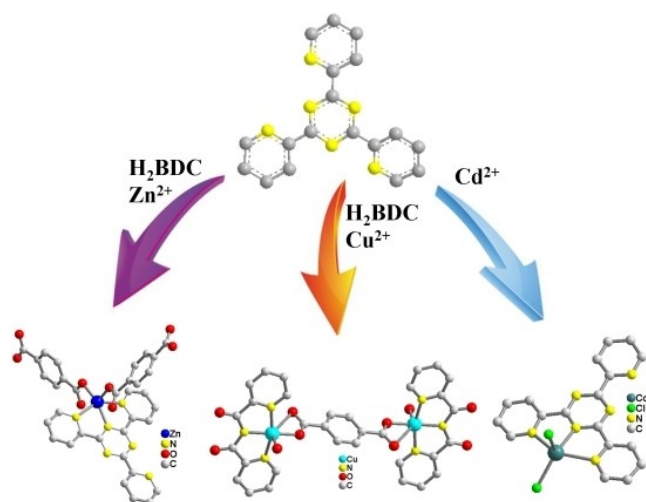   E-mail: chuhb@imu.edu.cn
[b] Y. Zhao
     Inner Mongolia Vocational College of Chemical Engineering
     Hohhot 010070 (P. R. China)
[c] S. Yuan
     Hohhot Natural Resources Comprehensive Survey Center
     China Geological Survey
     Hohhot 010010 (P. R. China)
[d] X. Zhang
     College of Science
     Inner Mongolia Agricultural University
     Hohhot 010018 (P. R. China)
     E-mail: lxyzxq@imau.edu.cn

ChemistryOpen

Research Article
doi.org/10.1002/open.202200176

Chemistry Europe
European Chemical
Societies Publishing

Scheme 1. Structures of the three crystal complexes.

due to their exposed amino groups and pores, while Cu-MOF displayed very poor adsorption property. Because CR contains two amino groups while the other three dyes contain none, CR is strongly and selectively adsorbed by forming hydrogen bonds with amino groups on Cd-MOF.

Results and Discussion

The synthesis of MOFs, infrared spectra of the ligands and MOFs (Figure S1), and crystallographic data and structure refinement information (Table S1–S4) are included in Supporting Information.

Crystal structure of Cd-MOF

In Cd-MOF, the central Cd^{2+} ion is coordinated by the TPTZ and Cl^- ligands. The crystal belongs to the monoclinic system with the space group $P2_1/c$. Scheme 1 shows the coordination environment of Cd^{2+} ion, and Figure 1 shows the cell packing diagram and the coordination polyhedron structure of the complex. The asymmetric unit is composed of one Cd^{2+}, one TPTZ, and two coordinated Cl^-. Without BDC^{2-}, Cl^- participates in the coordination, and TPTZ coordinates in the tridentate chelate form. With a coordination number of 5, the three
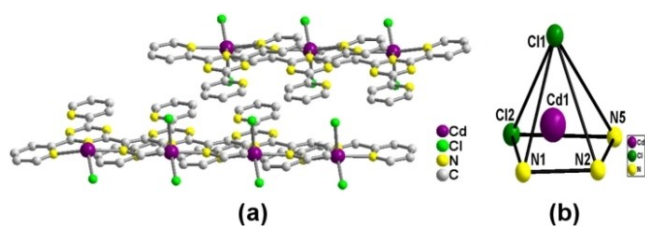
coordinated N atoms (N1, N2, and N5) of TPTZ and two coordinated Cl^- ions form a tetragonal pyramid around Cd^{2+}. The crystallographic refinement data are shown in Table S1, and selected bond lengths and bond angles are listed in Table S2. The three Cd–N bond lengths are 2.425(5) Å for Cd–N(1), 2.296(5) Å for Cd–N(2), and 2.469(5) Å for Cd–N(5), with N(2) located closer to Cd atom than N(1) or N(5).

Crystal structure of Zn-MOF

Zn-MOF is a polymer composed of Zn^{2+}, TPTZ, and BDC^{2-}. The crystal system is monoclinic and belongs to the $P2_1/c$ space group. Scheme 1 and Figure 2 show the crystal structure, cell packing diagram, and coordination polyhedron of Zn-MOF. The asymmetric unit is composed of one Zn^{2+} ion, one TPTZ, and one BDC^{2-}. The BDC^{2-} ligand links the monomers together to form a one-dimensional zigzag chain structure. From the figures, Zn^{2+} is coordinated to six atoms that form an octahedral structure. BDC^{2-} is coordinated through the bidentate chelate form of $[\kappa^2-\mu_2]$ and monodentate bridging coordination mode of $[(\kappa^1-\kappa^1)-\mu_2]$. The crystal refinement data are listed in Table S1, and selected bond lengths and angles are listed in Table S3. The three Zn–N bond lengths are 2.230(4) Å for Zn–N(1), 2.061(3) Å for Zn–N(2), and 2.250(3) Å for Zn–N(5). Similar to Cd-MOF, the Zn–N(2) bond length is also shorter than the other two.

Crystal structure of Cu-MOF

In the structural unit of Cu-MOF, two Cu^{2+} ions are coordinated by two PCA^-, one BDC^{2-}, and two water molecules (Scheme 1 and Figure 3). The two Cu^{2+} ions have the same coordination environment and are bridged by one BDC^{2-}. The crystal belongs to the monoclinic system with the space group $P2_1/c$. TPTZ is oxidised and hydrolysed to form 2-formyl pyridine amine (PCA^-), and neither O atoms of PCA^- coordinates with Cu^{2+}. The coordination number of Cu^{2+} is 6, through three N atoms in PCA^- (N1, N2, and N3), two O atoms of BDC^{2-} (O3 and O4), and one O atom (O5) of coordinated water. The coordination structure is an elongated octahedron. The crystallographic
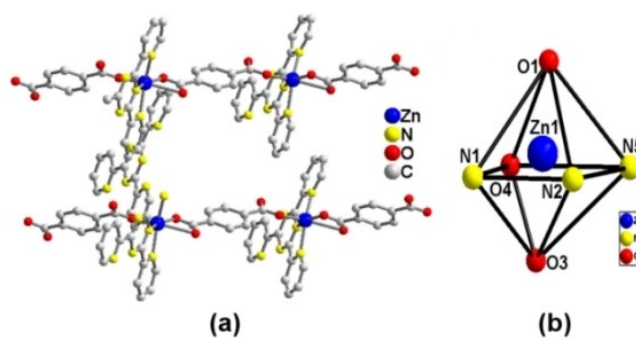

Figure 1. (a) Crystal cell packing diagram and (b) coordination polyhedron of Cd-MOF.
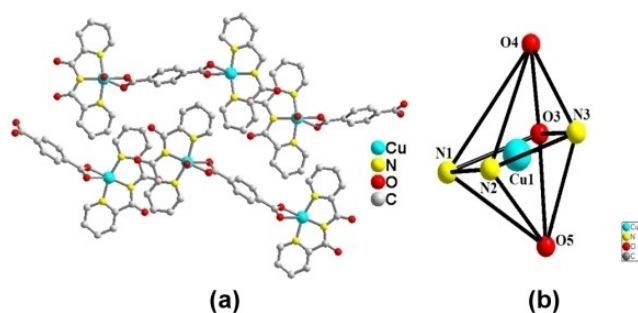

Figure 2. (a) Crystal cell packing diagram and (b) coordination polyhedron of Zn-MOF.

ChemistryOpen

Research Article
doi.org/10.1002/open.202200176

**Chemistry
Europe**
European Chemical
Societies Publishing

Figure 3. (a) Crystal cell packing diagram and (b) coordination polyhedron of Cu-MOF.

Figure 4. UV-vis spectra of (a) CR, (c) CR+MO, and (d) CR+RB solutions during adsorption by Cd-MOF. Inset photographs: colour of the dye solution before and after adsorption. (b) Concentration of CR versus time.

refinement data are shown in Table S1, and the selected bond lengths and bond angles are listed in Table S4. The lengths of the three Cu–N bonds are 2.004(9) Å for Cu–N(1), 1.932(7) Å for and Cu–N(2), and 1.997(8) Å for Cu–N(3). Similar to Cd-MOF and Zn-MOF, the bond length of Cu–N(2) is shorter than those of Cu–N(1) and Cu–N(3). Between the three Cu–O bonds, Cu–O(5) connected to the coordinated water is longer than Cu–O(3) connected to BDC^{2-}.

Adsorption of dye molecules on MOFs

Figure S2 depicts the structures of four dye molecules as well as the standard curve of CR. The four dyes CR, RB, MO, and MB mainly absorb in the wavelength regions of 400–600, 500–600, 400–550, and 550–700 nm, with peak absorption at 500, 560, 460, and 600 nm, respectively.

We next applied the three synthesised MOFs to the adsorption of these dyes in aqueous solution, either singly or in combination (CR+MO, CR+RB, and MB+MO+RB). The experiments were carried out at room temperature under continuous stirring, using 20 mL of dye solution containing a total of 1.25×10^{-4} mol L^{-1} dye molecules. The amount of adsorbent was 5 mg for Cd-MOF, 10 mg for Zn-MOF and 10 mg for Cu-MOF, respectively. After a given contact time, the solution was sampled by centrifuging, and UV-vis absorption was measured using a spectrometer. The UV-vis absorption spectra of CR, CR+MO, and CR+RB with Cd-MOF are shown in Figure 4; those of RB, MO, MB, and CR+MO+MB with Cd-MOF are shown in Figures S3–S4, and those of CR, CR+MO, CR+RB, RB, and MO with Zn-MOF are shown in Figure S5. From the results, CR alone or in a dye mixture could adsorb on Cd-MOF or Zn-MOF. Meanwhile, Cu-MOF did not adsorb any dye in the pure form or in mixtures, and therefore it will be excluded from further adsorption experiments.

According to Figures 4a and 4b, Cd-MOF rapidly lowered the absorbance of CR solution from 1.8 to 0.1 after the first 10 s, and further to nearly 0 at 20 s. This corresponds to reducing the CR concentration from 1.2×10^{-4} mol L^{-1} to close to 0. In the photographs, the CR solution quickly faded from bright red to colourless. Therefore, Cd-MOF rapidly removed most of the CR within 10 s and eliminated it within 20 s. When we tested mixed
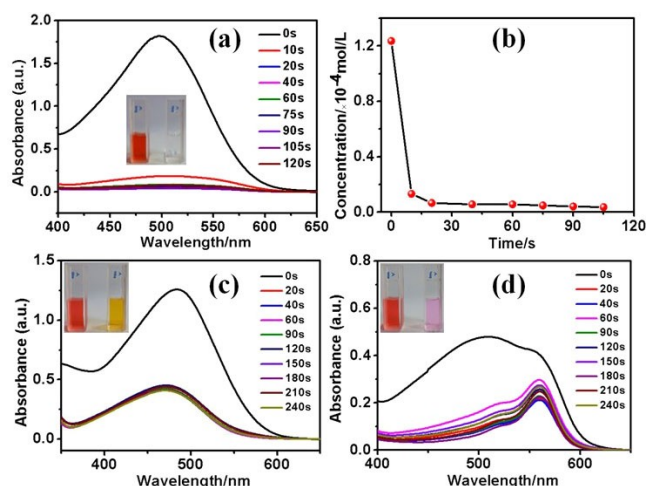
dyes containing CR (CR+MO and CR+RB), Figures 4c and 4d show that the solution colour changed after about 20 s, although there remained a strong UV absorption peak at about 460 and 560 nm that coincides with the characteristic absorption of MO and RB, respectively. These results indicate that Cd-MOF can selectively remove CR from aqueous solutions of mixed dyes.

Compared to Cd-MOF, the adsorption of CR on Zn-MOF was slower. In Figures S5a and S5b, Zn-MOF reduced the absorbance of CR solution from 1.80 to 0.72 after 40 s, corresponding to a concentration reduction from 1.2×10^{-4} to nearly 5×10^{-5} mol L^{-1}. When the contact time was extended to 3 min, both the UV absorption and CR concentration slowly declined to almost 0, and the solution became colourless. Hence, a large portion of CR was adsorbed by Zn-MOF within 40 s, and it was completely removed after 3 min. Figures S5c and S5d also show that in mixed solutions of CR+MO and CR+RB, Zn-MOF adsorbed CR but only negligible amount of MO and RB.

We also tested CR adsorption on Cd-MOF after different times and under varying pH conditions. The corresponding UV-vis spectra are shown in Figure S6. Cd-MOF has good adsorption performance in a wide pH range from 4–12, however the results at neutral pH are generally better than those at strongly acidic or basic conditions.

CR adsorption capacity of Cd-MOF and Zn-MOF

The equilibrium adsorption capacity is defined by Equation (1):[9,39]

$$Q_{eq} = \frac{c_0 - c_{eq}}{m} V \qquad (1)$$

where Q_{eq} (mg g^{-1}) is the amount of CR adsorbed on MOF at equilibrium, c_0 (mg L^{-1}) is the initial CR concentration, c_{eq}

ChemistryOpen

Research Article
doi.org/10.1002/open.202200176

Chemistry Europe
European Chemical
Societies Publishing

$(mg\,L^{-1})$ is the CR concentration at equilibrium, V (L) is the volume of CR aqueous solution, and m (g) is the weight of adsorbent. According to the above equation, the Q_{eq} value for Cd-MOF and Zn-MOF for CR is 348.4 and 174.2 $mg\,g^{-1}$, respectively.

We also explored the time-dependent adsorption capacity. Experimental results show that the adsorption capacity of 5 mg Cd-MOF after 3 min is 720 $mg\,g^{-1}$ (Figure 5b), and that after 5 min is 1440 $mg\,g^{-1}$ (Figure 5c). Figure 5d shows that when the adsorption capacity reached 1440 $mg\,g^{-1}$, the centrifuged supernatant is very clear due to the complete removal of CR. Table S5 compares the maximum adsorption capacity of CR on Cd-MOF and other reported porous materials. Cd-MOF is capable of adsorbing the largest amount of CR in the shortest time. Notably, the performance of Cd-MOF exceeds most CR adsorption capacities from the literature.[40–43]

Adsorption mechanism

The adsorption rate of dye depends on the contact between adsorbent and dye molecules and the diffusion of dye molecules.[44–45] To further explore the mechanism of CR adsorption on Cd-MOF, we measured the kinetic data and fitted them to three kinetic models (pseudo-first-order, pseudo-second-order, and intra-particle diffusion).[46–50] Figures S7a–S7c
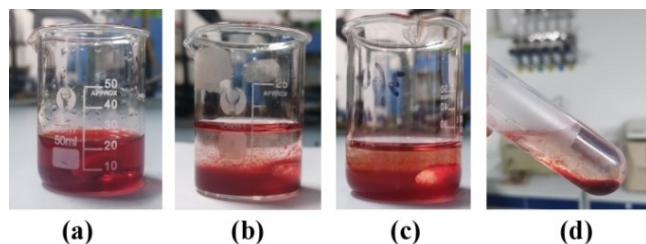

Figure 5. Colour changes of CR solution (a) before adsorption, (b) after 3 min (adsorption capacity: 720 $mg\,g^{-1}$), (c) after 5 min (adsorption capacity: 1440 $mg\,g^{-1}$), and (d) after centrifugation.
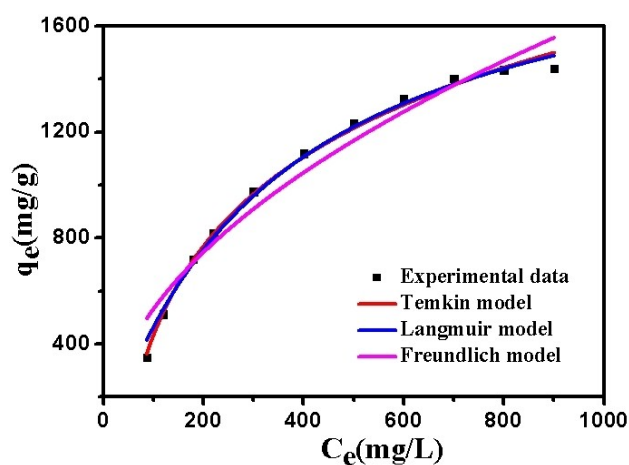

Figure 6. Langmuir, Freundlich, and Temkin adsorption isotherms of CR adsorption on Cd-MOF at room temperature.

plot $\log(q_e-q_t)$ vs. t, t/q_t vs. t, and q_t vs. t, respectively. The corresponding model constants were calculated according to the equations, and the R^2 value were obtained. The pseudo-second-order model has the highest R^2 value, indicating that adsorption of CR on Cd-MOF is dominated by chemisorption.

The adsorption equilibria are usually described by adsorption isotherms. Here, we used the Langmuir, Freundlich, and Temkin models to fit the isotherms of CR adsorption on Cd-MOF at room temperature (Figure 6). The calculated Langmuir parameters (K_L and q_{max}), Freundlich parameters (K_F and 1/n), and Temkin parameters (A_T and B) are presented in Table S5. The Temkin model yielded the best fit ($R^2 = 0.9957$). According to this model, adsorption of CR on Cd-MOF occurs through a hybrid of monolayer and multilayer mechanisms.

The adsorption rate and capacity in this study varied considerably according to the dye and adsorbent. From Figure S2, CR contains two NH_2 groups while the other three dyes contain none. Both Cd-MOF and Zn-MOF contain exposed amino groups (N3, N4, and N6 atoms from TPTZ) in addition to the pores, but Cu-MOF has neither. In addition, Cd^{2+} in Cd-MOF is coordinatively unsaturated with a coordination number of 5 (Scheme 1, Figure 1), which decreases the steric hindrance to adsorption. These structural features could explain the following experimental results: (1) Cu-MOF has no adsorption capacity, (2) Cd-MOF and Zn-MOF primarily adsorb CR and only a small amount of RB but not MO, (3) Cd-MOF has much larger CR adsorption rate and capacity compared to Zn-MOF, and (4) CR adsorption on Cd-MOF is mainly chemisorption. We speculate that CR adsorption on Cd-MOF may occur through two modes. One is by forming hydrogen bonds between the amino groups of CR and the exposed N from TPTZ on the adsorbent. The other is the direct coordination of amino groups in CR to Cd^{2+}, due to the lower steric hindrance and unsaturated coordination of Cd-MOF. In the case of Zn-MOF, CR adsorption should mainly occur through hydrogen bonds. The reason is that Zn^{2+} in the complex already have saturated coordination (coordination number = 6), and therefore CR could only adsorb on the exposed amino groups from TPTZ. Meanwhile, both the lack of exposed amino groups in Cu-MOF and the saturated coordination of Cu^{2+} inhibit CR adsorption. Nevertheless, the above hypotheses required further experimental verification.

Conclusions

Three crystalline metal complexes were prepared by a solvothermal method, using Cd^{2+}, Zn^{2+}, and Cu^{2+} as metal ions and TPTZ and BDC^{2-} as ligands. The composition and structure of the resultant coordination polyhedron depends on not only the ligands but also the metal ions. Because Cu has variable oxidation states, TPTZ is oxidised and hydrolysed to form PCA^-. Meanwhile, Cd^{2+} and Zn^{2+} do not have this effect. The exposed amino groups and pores likely enabled the selective adsorption of CR on Cd-MOF and Zn-MOF, although the adsorption behaviour is substantially different between the two. In addition, the lower steric hindrance posed by Cd-MOF

ChemistryOpen

Research Article
doi.org/10.1002/open.202200176

Chemistry
Europe
European Chemical
Societies Publishing

compared to Zn-MOF improved the CR adsorption rate and capacity. Moreover, Cd-MOF can adsorb CR in a wide pH range, and the adsorption capacity is up to 1440 mg g^{-1}. Such a material displaying fast and selective adsorption of organic dyes at high capacity could be useful in wastewater treatment.

Experimental Section

Chemical reagents and instrument: The purity of TPTZ was 98.5%. $CuCl_2 \cdot 2H_2O$, $CdCl_2 \cdot 2.5H_2O$, $ZnCl_2 \cdot 7H_2O$, H_2BDC, and other reagents were all of analytical grade and used as received. Elemental analysis of C, H, and N was performed on a Vario EL Cube elemental analyser (Hanau, Germany). Infrared spectra were recorded with KBr pellets on a Nicolet Nexus 670 Fourier-transform infrared spectrometer (Madison, WI, USA) within the spectral range of 4000–400 cm^{-1}. Crystal X-ray diffraction patterns were recorded at 293 K on an Xcalibur Eos Gemini diffractometer (South San Francisco, CA, USA) using a monochromator and Cu Kα radiation ($\lambda = 1.54184$ Å). UV-vis absorption spectra were recorded at room temperature on a Lambda 750 spectrometer (Perkin Elmer, USA).

Determination of crystal structure: Crystal data of the three MOFs were collected using an Xcalibur Eos Gemini diffractometer and a Cu Kα incident radiation beam. The structures were solved by direct methods and refined by full-matrix least-squares methods against F^2 with SHELXTL-97. The Diamond software was used to draw the crystal structures. All non-hydrogen atoms were refined with anisotropic thermal parameters, and all hydrogen atoms were omitted for the sake of clarity.

Deposition Numbers 1409195 (for Cd-MOF), 1062074 (for Zn-MOF), 1035072 (for Cu-MOF) contain the supplementary crystallographic data for this paper. These data are provided free of charge by the joint Cambridge Crystallographic Data Centre and Fachinformationszentrum Karlsruhe Access Structures service.

Selective adsorption of organic dyes: Based on the composition and structure of the three porous MOFs, we probed their ability to adsorb four organic dyes from water, namely methyl orange (MO), rhodamine B (RB), methylene blue (MB), and Congo red (CR), either singly or in equimolar mixtures (CR + MO, CR + RB, and MB + MO + RB) at the total dye concentrations of 1.25×10^{-4} mol L^{-1}. The dye adsorption rate and capacity of the three MOFs were determined. In a typical experiment, 5 mg of Cd-MOF or 10 mg of Zn-MOF was added to 20 mL of dye solution at room temperature. After stirring for a specific time, the dye concentration was measured by UV-vis absorption at specific wavelengths, with water as reference. Then, the adsorption rate and capacity were calculated.

Conflict of Interest

The authors declare no conflict of interest.

Data Availability Statement

Data available in article supplementary material.

[1] M. T. Uddin, M. A. Islam, S. Mahmud, M. Rukanuzzaman, *J. Hazard. Mater.* **2009**, *164*, 53–60.
[2] D. Mahanta, G. Madras, S. Radhakrishnan, S. Patil, *J. Phys. Chem. B* **2008**, *112*, 10153–10157.
[3] J. Ma, F. Yu, L. Zhou, L. Jin, M. X. Yang, J. S. Luan, Y. H. Tang, H. B. Fan, Z. W. Yuan, J. H. Chen, *ACS Appl. Mater. Interfaces* **2012**, *4*, 5749–5760.
[4] A. S. Patra, S. Ghorai, S. Ghosh, B. Mandal, S. Pal, *J. Hazard. Mater.* **2016**, *301*, 127–136.
[5] S. Boumaza, F. Kaouah, D. Hamane, M. Trari, S. Omeiri, Z. Bendjama, *J. Mol. Catal. A* **2014**, *393*, 156–165.
[6] V. S. Mane, P. V. V. Babu, *Desalination* **2011**, *273*, 321–329.
[7] W. Wei, R. J. Xie, Y. F. Zhang, X. Bai, L. Gu, R. Da, X. Y. Liu, *J. Mater. Chem. A* **2015**, *3*, 4314–4322.
[8] S. Sansuk, S. Srijaranai, S. Srijaranai, *Environ. Sci. Technol.* **2016**, *50*, 6477–6484.
[9] X. Q. Zhang, Y. F. Gao, H. T. Liu, Z. L. Liu, *CrystEngComm* **2015**, *17*, 6037–6043.
[10] J. Y. Xiao, H. Zhang, Y. Xia, Z. L. Li, W. Huang, *RSC Adv.* **2016**, *6*, 39861–39869.
[11] D. Maiti, S. Mukhopadhyay, P. S. Devi, *ACS Sustainable Chem. Eng.* **2017**, *5*, 11255–11267.
[12] N. C. Zheng, Z. Wang, J. Y. Long, L. J. Kong, D. Y. Chen, Z. Q. Liu, *J. Colloid Interface Sci.* **2018**, *525*, 225–233.
[13] N. Mohammad, B. Hayati, M. Arami, C. Lan, *Desalination* **2011**, *268*, 117–125.
[14] J. E. Aguiar, J. A. Cecilia, P. A. S. Tavares, D. C. S. Azevedo, E. R. Castellón, S. M. P. Lucena, I. J. Silva Junior, *Appl. Clay Sci.* **2017**, *135*, 35–44.
[15] J. Q. Zhao, Z. X. Lu, X. He, X. F. Zhang, Q. Y. Li, T. Xia, W. Zhang, C. H. Lu, *ACS Sustainable Chem. Eng.* **2017**, *5*, 7723–7732.
[16] T. Maneerung, J. Liew, Y. Dai, S. Kawi, C. Chong, C. H. Wang, *Bioresour. Technol.* **2016**, *200*, 350–359.
[17] T. Yamamoto, Y. H. Kim, B. C. Kim, A. Endo, N. Thongprachan, T. Ohmori, *Chem. Eng. J.* **2012**, *182*, 443–448.
[18] Y. Zhang, S. Xu, H. H. Zhou, H. C. Qi, H. G. Wang, *J. Solid State Chem.* **2021**, *293*, 121801–121812.
[19] S. H. Wei, A. R. Kamali, *J. Alloys Compd.* **2021**, *886*, 161201–161215.
[20] S. Zhao, Y. Wen, C. Du, T. Tang, D. Kang, *Chem. Eng. J.* **2020**, *402*, 126180–126192.
[21] A. Molla, Y. Li, B. Mandal, S. G. Kang, S. H. Hur, J. S. Chung, *Appl. Surf. Sci.* **2019**, *464*, 170–177.
[22] M. Hasanzadeh, A. Simchi, H. S. Far, *J. Ind. Eng. Chem.* **2020**, *81*, 405–414.
[23] P. Qin, D. Chen, M. Y. Li, *J. Mol. Liq.* **2022**, *359*, 119231–119241.
[24] H. S. Far, M. Hasanzadeh, M. Najafi, R. Rahimi, *ChemistrySelect* **2022**, *7*, e202104191.
[25] G. S. Hu, G. Cui, J. Zhao, M. Y. Han, R. Y. Zou, *Polym. Chem.* **2022**, *13*, 3827–3832.
[26] F. Zhang, F. L. Bei, J. M. Cao, *J. Chem. Crystallogr.* **2008**, *38*, 561–565.
[27] K. Abdi, H. Hadadzadeh, M. Weil, H. A. Rudbari, *Inorg. Chem. Acta* **2014**, *416*, 109–121.
[28] F. P. Huang, J. L. Tian, G. J. Chen, D. D. Li, W. Gu, X. Liu, S. P. Yan, D. Z. Liao, P. Cheng, *CrystEngComm* **2010**, *12*, 1269–1279.
[29] Z. Hasan, S. H. Jhung, *J. Hazard. Mater.* **2015**, *283*, 329–339.
[30] J. P. Li, J. Z. Fan, D. Z. Wang, *J. Solid State Chem.* **2016**, *239*, 251–258.
[31] C. C. Du, J. Z. Fan, X. F. Wang, S. B. Zhou, D. Z. Wang, *J. Mol. Struct.* **2017**, *1133*, 348–357.

[32] K. J. Chen, R. B. Lin, P. Q. Liao, C. T. He, J. B. Lin, W. Xue, Y. B. Zhang, J. P. Zhang, X. M. Chen, *Cryst. Growth Des.* **2013**, *13*, 2118–2123.

[33] C. Daiguebonne, N. Kerbellec, K. Bernot, Y. Gérault, A. Deluzet, O. Guillou, *Inorg. Chem.* **2006**, *45*, 5399–5406.

[34] X. D. Guo, G. S. Zhu, F. X. Sun, Z. Y. Li, X. J. Zhao, X. T. Li, H. C. Wang, S. L. Qiu, *Inorg. Chem.* **2006**, *45*, 2581–2587.

[35] A. Das, C. Marschner, J. Cano, J. Baumgartner, J. Ribas, M. Salah El Fallah, S. Mitra, *Polyhedron* **2009**, *28*, 2436–2442.

[36] N. Goel, U. P. Singh, *J. Phys. Chem. A.* **2013**, *117*, 10428–10437.

[37] N. Lopez, H. Zhao, D. Zhao, H.-C. Zhou, J. P. Riebenspies, K. R. Dunbar, *Dalton Trans.* **2013**, *42*, 54–57.

[38] H. Hadadzadeh, M. Maghami, J. Simpson, A. D. Khalaji, K. Abdi, *J. Chem. Crystallogr.* **2012**, *42*, 656–667.

[39] Y. C. He, J. Yang, W. Q. Kan, J. F. Ma, *CrystEngComm* **2013**, *15*, 848–851.

[40] W. Q. Cai, Y. Z. Hu, J. Chen, G. X. Zhang, T. Xia, *CrystEngComm* **2012**, *14*, 972–977.

[41] L. Cheng, L. Zhang, H. X. Wang, F. X. Song, *Korean J. Chem. Eng.* **2022**, *39*, 1257–1267.

[42] J. Fei, Y. Cui, X. Yan, W. Qi, Y. Yang, K. Wang, Q. He, J. Li, *Adv. Mater.* **2008**, *20*, 452–456.

[43] C. Yu, X. Dong, L. Guo, J. Li, F. Qin, L. Z. Zhang, J. Shi, D. Yan, *J. Phys. Chem. C* **2008**, *112*, 13378–13382.

[44] S. Ghorai, A. Sarkar, M. Raoufi, A. B. Panda, H. Schönherr, S. Pal, *ACS Appl. Mater. Interfaces* **2014**, *6*, 4766–4777.

[45] L. Liu, Z. Y. Gao, X. P. Su, X. Chen, L. Jiang, J. M. Yao, *ACS Sustainable Chem. Eng.* **2015**, *3*, 432–442.

[46] N. F. Al-Harby, E. F. Albahly, N. A. Mohamed, *Polymer* **2022**, *14*, 271–299.

[47] Y. Yao, B. He, F. Xu, X. Chen, *Chem. Eng. J.* **2011**, *170*, 82–89.

[48] H. Chen, J. Zhao, J. Wu, G. Dai, *J. Hazard. Mater.* **2011**, *192*, 246–254.

[49] Y. S. Ho, G. McKay, *Process Biochem.* **1999**, *34*, 451–465.

[50] P. K. Obulapuram, T. Arfin, F. Mohammad, S. K. Khiste, M. Chavali, A. N. Albalawi, H. A. Al-Lohedan, *Polymer* **2021**, *13*, 3490–3506.